



Photodeposited Pd nanoparticle catalysts supported on photoactivated TiO₂ nanofibers

Emilly A. Obuya^a, William Harrigan^a, Dickson M. Andala^a, Jennifer Lippens^b, Thomas C. Keane^b, Wayne E. Jones Jr.^{a,*}

^a Department of Chemistry, State University of New York at Binghamton, 4400 Vestal Parkway East, Vestal, NY 13902, USA

^b Department of Chemistry and Biochemistry, Russell Sage College, 65 First Street, Troy, NY 12180, USA

ARTICLE INFO

Article history:

Received 28 January 2011

Received in revised form 23 March 2011

Accepted 24 March 2011

Available online 31 March 2011

Keywords:

Electrospinning

Heterogeneous catalysis

Nanofibers

Nanoparticles

Catalyst supports

Heck reaction

ABSTRACT

Pd nanoparticle catalysts supported on photoactive titania nanofibers were investigated and evaluated with respect to model C–C coupling reactions. Titania nanofibers were prepared via the electrospinning technique, followed by in situ formation of the Pd nanoparticles catalyst on the TiO₂ support. Pd nanoparticles of between 2 and 5 nm were successfully stabilized on the surface of electrospun nanofibers which had diameters between 150 ± 50 nm. The new catalyst was found to have increased surface area and improved catalytic functions compared to commercially available materials or other Pd–TiO₂ catalysts produced by different modes of synthesis. The activity and selectivity of 0.05 mol% Pd–TiO₂ catalyst in the Heck reaction has been investigated with a careful look into the nature of starting materials and products under varying conditions of temperature, solvent and base. The catalyst was found to be highly active under air atmosphere with reaction temperatures of up to 160 °C. Optimized reaction conditions resulted in a 98% yield of trans-stilbene for the iodobenzene–styrene system with a TOF value of 7.85 min⁻¹.

© 2011 Elsevier B.V. All rights reserved.

1. Introduction

Catalysis is a multi-billion dollar industry that accounts for production of 60% of all the chemicals currently being used for most chemical processes worldwide [1,2]. Some of the products derived from catalytic processes include polymers, plastics, pharmaceuticals and detergents. Synthesis of these products predominantly involves C–C coupling reactions, a variety of which have been reported in the literature [3–6]. The Heck reaction, which is a Pd-catalyzed C–C coupling reaction employed in organic synthesis, is well established in the literature and utilizes readily available starting materials with mild reaction conditions [7]. Homogenous Heck catalysis, which typically involves the use of Pd complexed to a phosphine ligand, is by far superior to heterogeneous systems in the conversion of the readily available but rather inactive aryl bromides and aryl chlorides [8–11]. However, the phosphine ligands are highly air-sensitive and make it very difficult to recover the catalyst from the reaction matrix [12]. This hinders catalyst recovery and increases the levels of pollution from the Pd metal wastes generated.

Heterogeneous catalysis seems to be the method of choice for most Heck C–C coupling reactions, the most frequent motivation

being the ease of recovery, recyclability and re-use of catalyst [13–16]. For heterogeneous catalysis, the problem of catalyst separation and recovery from the reaction matrix is addressed by using various catalyst supports to immobilize the Pd and provide a large enough surface area for catalysis without dissolution of Pd in the solution matrix [16,17]. Currently, the most active heterogeneous Pd systems include; (i) Silica-supported Pd complexes, with favorable Si–OH surface anchorage [15,18,19] (ii) Pd–C, with high specific surface area of the activated carbon [12,16,20] (iii) Pd–zeolites, with the cationic exchange properties of the mesoporous zeolites which allow for better retention of the ionic forms of Pd [5,21,22] and (iv) Pd–metal oxides, with the broad availability of metal oxide supports such as Al₂O₃, TiO₂, ZrO₂, ZnO etc. [16].

Metal oxides are the most lucrative Pd-support for heterogeneous catalysis based on their broad availability and cost effective modes of synthesis [11,23–25]. These metal oxides have increased photoactivities due to the photoinduced electron–hole pairs on their surfaces that can be harvested to enhance electron transfer and chemical reactivity. One of the most actively studied semiconductor materials is TiO₂, which is a transition metal oxide with band gap energies of between 3.0 and 3.2 eV [26]. The semiconducting nature of TiO₂ has made it possible for the utilization of UV–visible radiation to harvest conduction band electrons that are subsequently used to reduce metallic ions on the TiO₂ surface. [27] This paper explores the high thermal stability of TiO₂ in a nanofibrous form with a careful look into the development of simple,

* Corresponding author. Tel.: +1 607 777 2451; fax: +1 607 777 4478.

E-mail address: wjones@binghamton.edu (W.E. Jones Jr.).

low-cost, and stable catalysts. In this case, the photoactivity of the TiO₂ substrate can also be used to photodeposit the catalytic Pd nanoparticles to improve overall catalyst preparation.

Here we report the first example of photoenhanced Pd–TiO₂ catalysts by this method and the characterization of these materials. The resulting catalysts were evaluated using the representative Heck reaction as a model C–C coupling reaction. In particular, the catalytic reactivity was correlated with reaction parameters for the Pd–TiO₂ nanoparticle catalyst with the iodobenzene–styrene system. The activity of the new Pd–TiO₂ catalyst was compared to commercially available Pd–C, as well as similar metal oxide catalysts synthesized via non-photoactive modes of synthesis. While the nanofibrous nature of this new catalyst and the stabilization of the nanoparticles on the surface to prevent aggregation are clear advantages, the potential further enhancement of the catalyst by UV irradiation to take advantage of the optical properties of the TiO₂ were also investigated.

2. Experimental

2.1. Materials

Polymethylmethacrylate, (PMMA) Mw 350,000, titanium isopropoxide (TiP), palladium chloride (PdCl₂), ethylene glycol, polyvinyl pyrrolidone (PVP) N,N-dimethylformamide (DMF), N,N-dimethylacetamide (DMAc), N-methyl-2-pyrrolidone (NMP), methanol (MeOH), sodium carbonate (Na₂CO₃), sodium acetate (NaOAc), triethylamine (Et₃N), potassium carbonate (K₂CO₃), iodobenzene and styrene were purchased from Sigma Aldrich and used as received. Trichloromethane, hydrochloric acid and nitric acid were purchased from J.T Baker while the 6% hydrogen gas balanced with nitrogen was obtained from Airgas.

2.2. Instrumentation

The morphology and size of the titania nanofibers were observed using a Hitachi S-570 or Supra Zeiss 55VP SEM Model, equipped with an EDAX system for Energy Dispersive Spectroscopic analysis. TEM images were obtained from JEOL 2010 FETEM instrument. The TEM samples were dispersed in EtOH by sonication and the resulting solution placed on a lacey carbon grid, which was left in air to evaporate the solvent. The photodeposition experiments were performed using a UV (Spectroline Model ENF 240C, 115V) lamp irradiated at ~365 nm and placed approximately 15 cm away from the reacting solution.

FTIR was done using Bruker IR Model Equinox 55/digilab FTS-40 PRO, where a KBr pellet of electrospun fiber mat was spread on the IR holder and an IR beam passed through the pellet as is. The X-ray diffraction spectra were measured using a Scintag X-ray diffractometer with X-ray wavelength of 1.5418 Å (Cu Kα) radiation source. The samples for PXRD were compacted to at least 1 mm in thickness to prevent penetration of the X-ray beam.

GC–MS analysis of the Heck reaction aliquots was done on two different instruments to ensure accuracy of experimental results: From SUNY-Binghamton, analysis was done on a Varian 4000 GC-MS equipped with a Varian Factor-Four VF-5 MS Column. Selectivity and conversion values were obtained from MS peak areas relative to an external standard of known concentrations of pure iodobenzene and trans-stilbene. The column was programmed with a 3 min post injection hold time at 50 °C followed by a 25 °C/min ramp to 300 °C. The aliquots were fed into the GC using a Combi auto sampler at an injection temperature of 280 °C. From Russell Sage College, analysis was obtained from a Shimadzu QP-5050 GC-MS with an auto sampling tray which uses a micro syringe to inject 1 μL of the diluted sample into a Restek XTI-5 cap-

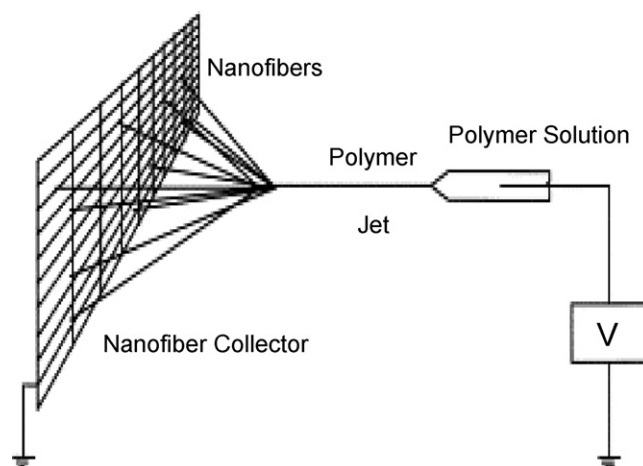


Fig. 1. Schematic representation of the electrospinning process [26].

illary column. Injections are made in split-less mode with a column flow rate of 1.0 mL/min. Uv–vis analysis of the aliquots was done on an 8452A Hewlett Packard Diode Array spectrophotometer, where absorbance measurements were taken of approximately 0.25 μL of each aliquot diluted with 4 mL methanol.

To test the amount of Pd²⁺ in solution during Heck catalysis, an ARL Fisons SS-7 DCP-AES with Pd emission peaks at 363.5 nm wavelength was used for Pd composition analysis. The organics in the aliquots were quenched in a concentrated aqua regia solution, followed by dilution in the range of 1–50 ppm in distilled water. Calibration curves were obtained from dissolved standards with concentrations of 0–50 ppm of the acid matrix.

For analysis of pure Heck reaction product, a small amount of purified sample was dissolved in CDCl₃ and ¹H-NMR spectra was recorded on a Bruker AM-360 spectrometer.

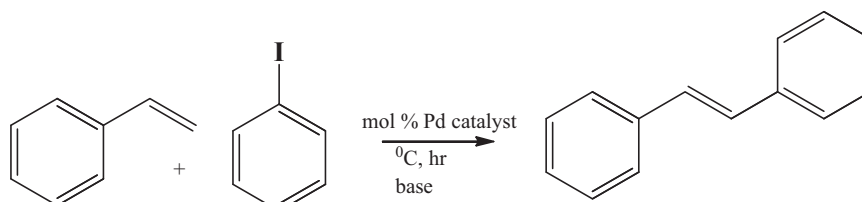
2.3. Synthesis of TiO₂ nanofibers

A 1:2 weight ratio of PMMA:TiP was prepared by completely dissolving 320 mg of PMMA in 2 mL chloroform followed by drop wise addition of 640 mg TiP with continuous stirring of the reaction mixture for complete dissolution. 2 mL DMF was added to increase the dielectric constant of the composite solution and hence enable the electrospinning process at a high KV Spellman SL 30 generator, Fig. 1.

A high electrical potential (25 kV/cm) was applied across the syringe needle and the collector screen where the PMMA/TiP solution was spun into composite nanofibers and deposited as a randomly oriented non-woven mat on the collector screen. These fibers were left overnight to allow for complete hydrolysis of the TiP to Ti(OH)₄, and subsequently subjected to calcination at 500 °C in air at a ramp rate of 10 °C/min for 1 h.

2.4. Photodeposition of Pd nanoparticles on TiO₂ nanofibers

A typical procedure involved heating a 10 mL solution of ethylene glycol in a 110 °C oil bath for 30 min, followed by addition of TiO₂ nanofibers with UV light irradiation for another 30 min under an inert atmosphere. Pd nanoparticles were then synthesized in situ on the electrospun TiO₂ surface via a modified polyol technique. Typically 5 wt.% Pd–TiO₂ was prepared by adding a 2:3 mole ratio of PdCl₂:PVP into the photo-illuminated TiO₂ fibers in the EG solution at 110 °C. On addition of the PdCl₂:PVP solutions, the UV lamp was turned off to allow for the nucleation of the Pd nanoparticles on the TiO₂ support surface. At the end of the reaction, the catalyst



Scheme 1. Heck reaction conditions.

was washed several times with acetone under centrifugation and dried at 120 °C for 3 h.

2.5. Heck reaction

Typically, 4.44 mmol iodobenzene, 7.23 mmol base, 5 mL solvent, 6.69 mmol styrene and 0.05 mol% Pd catalyst, as in Scheme 1, were introduced into a round bottomed flask and immersed into a pre-heated oil bath, thereby initiating the reaction. The reaction vessel was sealed with septum and maintained on reflux under atmospheric conditions. Aliquots of the reaction mixture were obtained at pre-determined intervals for further analysis which involved screening the catalyst for solvent, base, temperature and Pd leaching effects to achieve the optimized conditions for the Pd-TiO₂ catalyst activity.

3. Results and discussion

3.1. Catalyst preparation and characterization

The Pd-TiO₂ catalyst system was prepared as described above. The electrospinning process had previously been used to prepare nanofibrous supports [28]. The key modification to the procedure was to apply a UV light photoinduced electron transfer for the deposition of the Pd nanoparticles. The catalyst was collected, dried and purified prior to thorough characterization as outlined by the techniques below.

3.1.1. BET surface area analysis

Surface area for the Pd-TiO₂ catalyst material was determined by the BET method. The sample was heated at a temperature of 250 °C to remove any adsorbed moisture, followed by nitrogen adsorption/desorption isotherms against relative pressure at 77 K. The results from this experiment give a type IV isotherm indicating the porous nature of the nanostructured material, Fig. 2. The hysteresis loop suggests mesoporosity of these materials with pore condensation at high pressure. The BET surface area, calculated from the quantity of monolayer of nitrogen gas adsorbed, was determined to be ~422 m²/g for the TiO₂ nanofibers and ~93 m²/g for the Pd-TiO₂. The decrease in surface area of the TiO₂ nanofibers on loading the Pd nanoparticles is indicative of the filling of the pores on TiO₂ hence less available surface for nitrogen adsorption.

3.1.2. Scanning electron microscope

The PMMA/TiP composite fibers were smooth in morphology with average diameters ranging between 250 ± 100 nm. Calcination of the composite fibers in air at 500 °C selectively removed the PMMA resulting in TiO₂ nanofibers with diameters of 150 ± 50 nm, as in Fig. 3. The SEM image, Fig. 4, shows the porous nature of the TiO₂ nanofibers which is favorable for the nucleation of palladium nanoparticles.

3.1.3. Fourier transform infrared and thermogravimetric analysis

FTIR was used to confirm the removal of PMMA from the composite solution, the distinctive CH_x stretching and bending modes

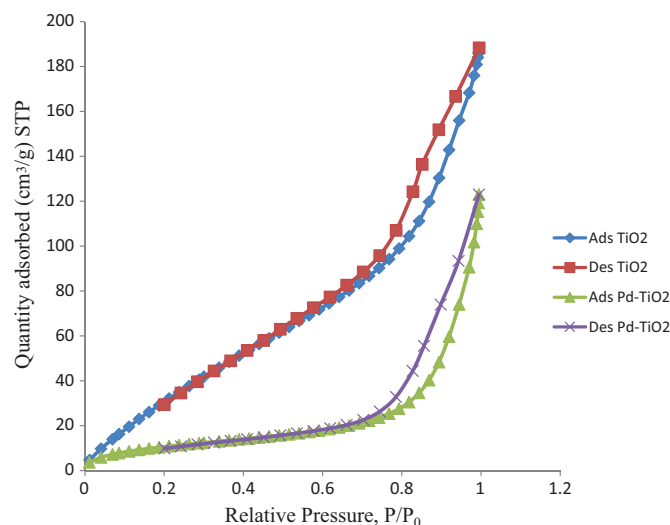


Fig. 2. Type IV Nitrogen adsorption–desorption isotherms for the BET surface area analysis of TiO₂ nanofibers and Pd-TiO₂ catalyst, indicative of the mesoporous nature of the nanostructured material.

(2994 cm⁻¹ and 2950 cm⁻¹) C=O stretch (1734 cm⁻¹), the asymmetric C–C–O stretch (1272 cm⁻¹ and 1245 cm⁻¹), the asymmetric C–O–C stretch (1194 cm⁻¹ and 1152 cm⁻¹) and the C–C skeletal stretch (752 cm⁻¹) are all missing from the analysis done after calcination at 500 °C, Fig. 5. This was indicative of the removal of PMMA leaving inorganic TiO₂, with a broad band associated with stretching and bending modes of ν(Ti–O) at 500–700 cm⁻¹. The average TiO₂ content from TGA analysis was found to be ~36.55%. This is consistent with the complete loss of PMMA which has a thermal decomposition temperature of 260–280 °C, Fig. 6.

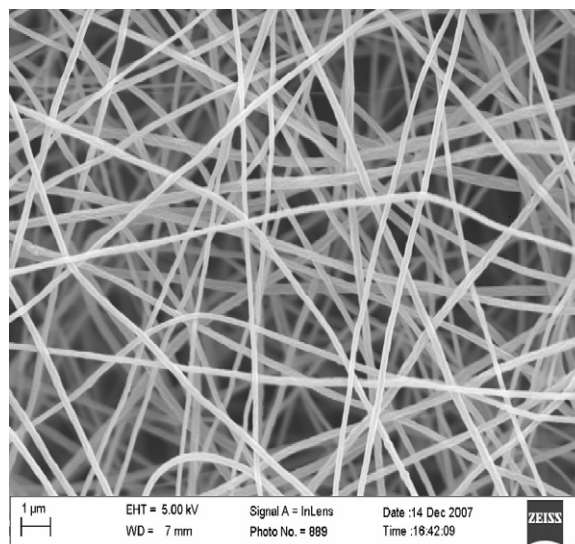


Fig. 3. SEM image of inorganic TiO₂ after calcination with 150 ± 50 nm diameter.

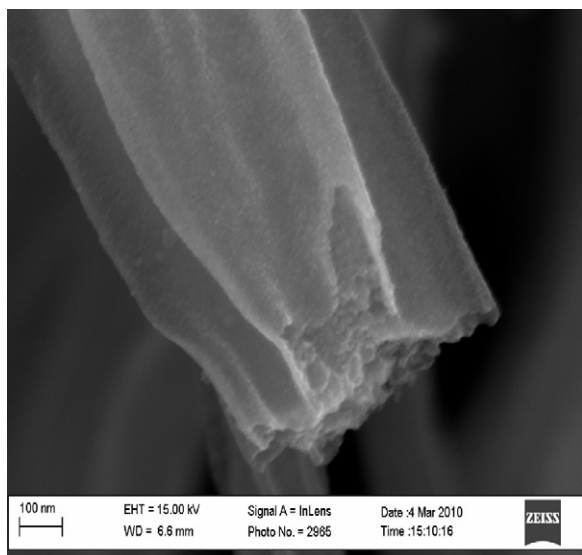


Fig. 4. Magnified image of the electrospun TiO_2 showing the smooth and porous nature of the fiber.

3.1.4. Powder X-ray diffraction analysis

PXRD analysis confirmed the TiO_2 nanofibers were in the anatase phase by comparison to standard diffractions from JCPDS card 21-1272. The diffraction peaks were indexed corresponding to those of anatase phase of titania $25.06^\circ(1\ 0\ 1)$, $38.14^\circ(1\ 0\ 3, 0\ 0\ 4, 1\ 1\ 2)$, $47.80^\circ(2\ 0\ 0)$, $54.42^\circ(2\ 1\ 1)$, $62.42^\circ(2\ 0\ 4)$, $69.62^\circ(1\ 1\ 6, 2\ 2\ 0)$, $75.14^\circ(2\ 1\ 5)$, Fig. 7.

3.1.5. Energy dispersive spectroscopy

EDS gives an elemental analysis of the sample, showing the presence and relative distribution of the elements present. The EDS spectrum, Fig. 8, obtained for the Pd– TiO_2 catalyst indicates successful deposition of the Pd nanoparticles on the electrospun Titania surface. The observed Ti and O peaks were consistent with the formation of TiO_2 nanofibers. The presence and overall percentage of Pd from the EDS spectrum was consistent with the deposition of 5 wt.% of Pd on the TiO_2 surface. The presence of the C peaks could be attributed to residual organics from the incomplete combustion of PMMA during calcination.

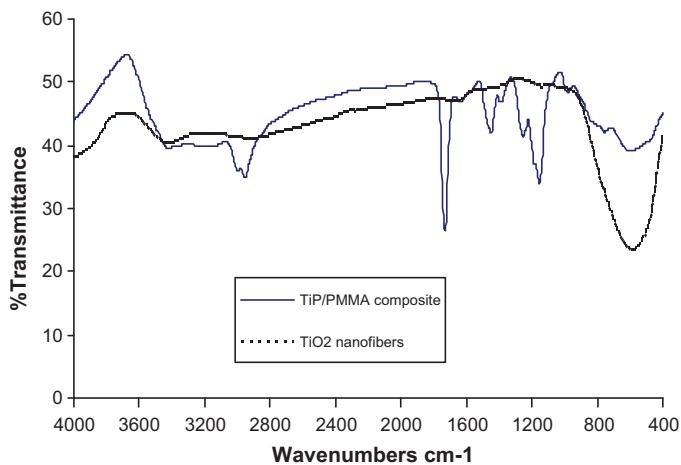


Fig. 5. FTIR spectrum of TiP/PMMA composite fibers before and after calcination showing complete removal of PMMA peaks after calcination.

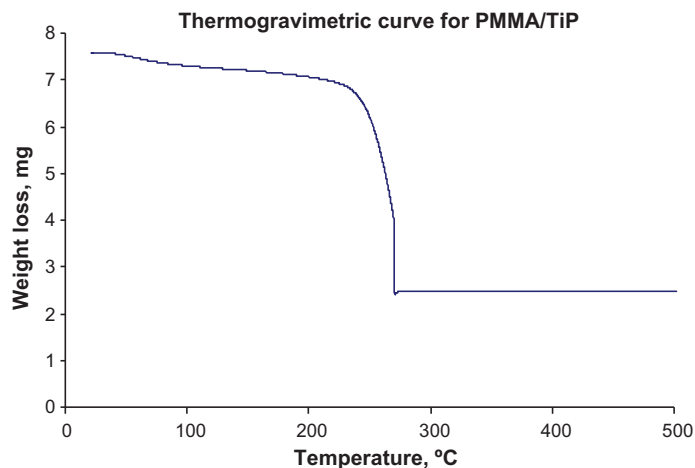


Fig. 6. Thermogravimetric profile for degradation of PMMA-TiP , showing thermal decomposition of PMMA at $260\text{--}280^\circ\text{C}$. Average TiO_2 content from this analysis was 36.55%.

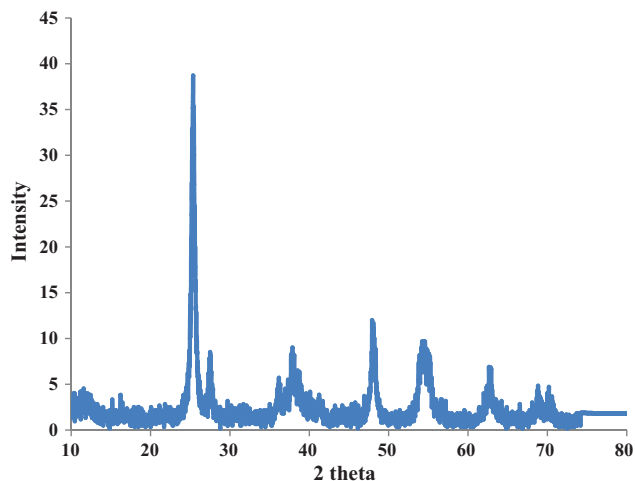


Fig. 7. Powder X-ray diffraction profile of TiO_2 nanofibers after calcination at 500°C , indicating the formation of the anatase phase of titania.

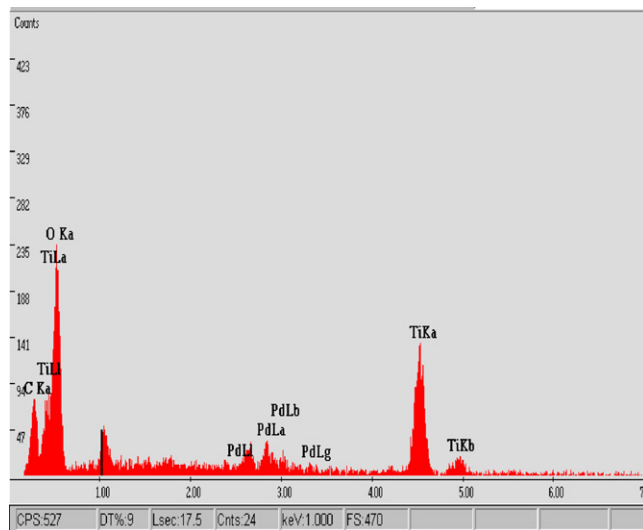


Fig. 8. EDS spectrum of Pd– TiO_2 , showing the presence of Pd, Ti and O; the absence of impurities from this spectrum indicates a successful technique for Pd deposition on the titania surface.

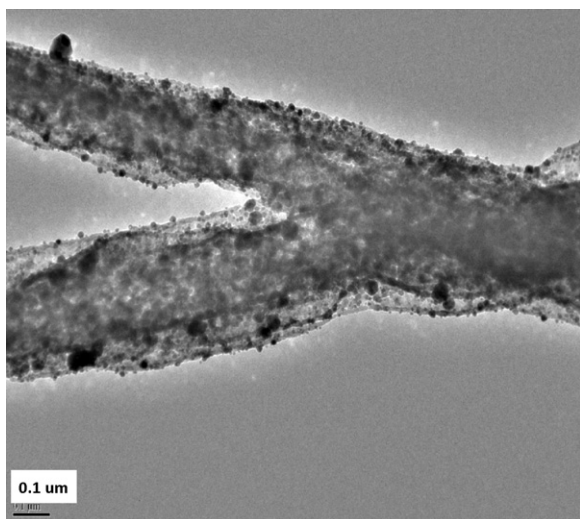


Fig. 9. TEM image of TiO₂ nanofibers showing a cross-section of the fiber with the darker spots corresponding to loading of Pd nanoparticles on the titania surface.

3.1.6. Transmission electron microscopy

Deposition of Pd nanoparticles was further studied by TEM analysis. A uniform loading of Pd nanoparticles on the titania fiber was observed with monodisperse Pd particles of between 2 and 4 nm particle sizes, **Figs. 9 and 10**. The TEM image was proof of the successful nucleation and particle growth on the porous TiO₂ surface without the use of organic stabilizers or special reaction conditions. For catalytic purposes, the electrospun TiO₂ provided a support matrix to anchor the Pd nanoparticles in place to avoid aggregation and thus maintain the high surface area required for conversion of the aryl chloride. The Pd nanoparticles were stabilized in place even after the Heck reaction mechanism thus allowing for efficient re-use in subsequent steps.

3.2. Catalyst application

3.2.1. Heck reaction

The catalytic cycle proposed by Heck, **Fig. 11**, involves the oxidative addition of an aryl halide to the co-ordinatively unsaturated Pd complex [17] and is characteristic of many C–C coupling reactions.

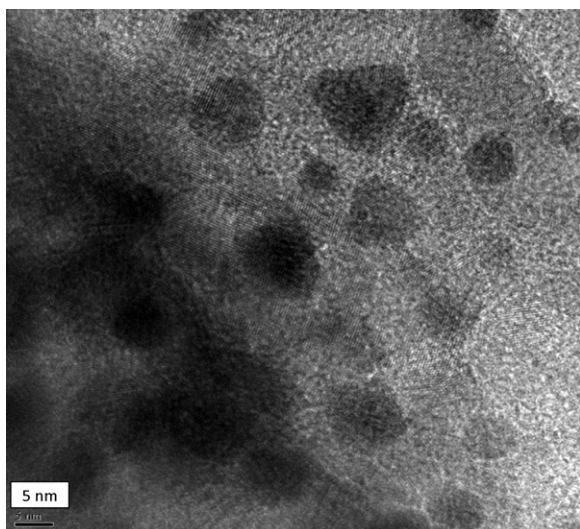


Fig. 10. TEM image of Pd–TiO₂ catalyst at higher magnification showing the diameter of the Pd nanoparticles to be ~5 nm.

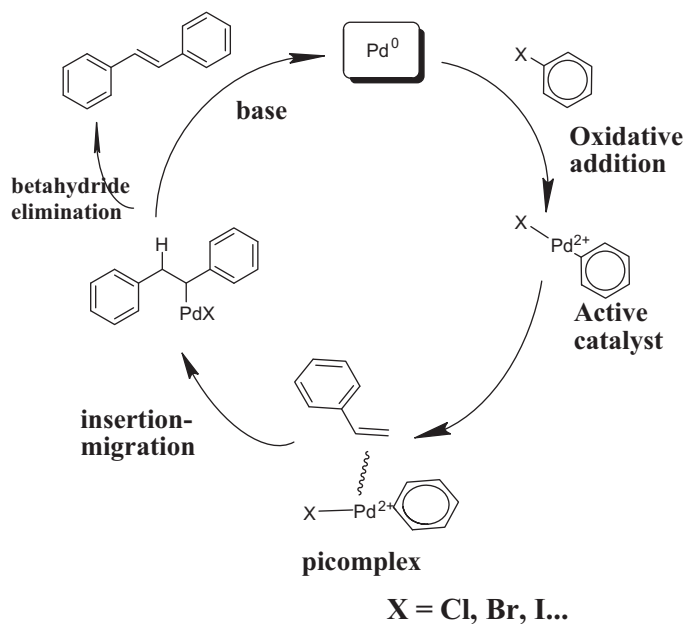


Fig. 11. Heck reaction mechanism.

A π complex is formed by association with an electron-rich alkene, leading to the formation of a new C–C bond. Beta-hydride elimination occurs to form product while releasing the catalyst complex. The catalytically active Pd species is regenerated in the presence of a base thereby recycled in a similar reaction cycle.

Initial studies were carried out using commercially available Pd–C catalysts as a control experiment. The results of Heck coupling can be compared with the newly prepared Pd–TiO₂ nanofiber catalyst in terms of activity and selectivity for the Heck reaction. The rate of product formation was monitored by drawing aliquots from the reaction mixture at pre-determined intervals, with a subsequent Uv–vis as well as GC–MS analysis of the product peaks.

3.2.2. GC–MS analysis of Heck reaction aliquots

GC data of reaction aliquots gave retention times and peak areas of Heck reactants and products with no formation of side products, **Fig. 12**. Typical peak areas obtained as in **Fig. 13**, were then used to calculate selectivity and conversion values compared to known concentrations of pure starting materials and desired product, **Fig. 14**. The mass spectrum of each aliquot had a molecular ion peak at m/z 180.1 and a base peak at 179.3, which was found to be closest to trans-stilbene through a library search.

The Pd–TiO₂ catalyst was found to be 100% selective for the desired product at 20 min reaction time whereas the commercial Pd–C catalyst achieved 100% selectivity at 60 min reaction time. The conversion values for Pd–TiO₂ recorded a steady rise with time up to a constant 83% conversion maximum. The results for the Heck reaction with Pd–C catalyst was 100% conversion at 60 min reaction time, but lower conversions of upto 79% with reaction progress, this indicates formation of side products hence instability of the Pd–C catalyst.

3.2.3. Uv–vis analysis of Heck reaction aliquots

In order to simplify the real time analysis of the catalyst reaction, it was possible to use Uv–vis spectroscopy to monitor the formation of product. A Uv–vis spectrum of pure stilbene shows four distinct absorbance peaks at 229 nm, 296 nm, 308 nm and 320 nm. The 296 nm peak, which can be assigned to a π – π^* transition, was ideal for monitoring the reaction as it had the most intense absorbance value and was found to have the least overlap with the reactant

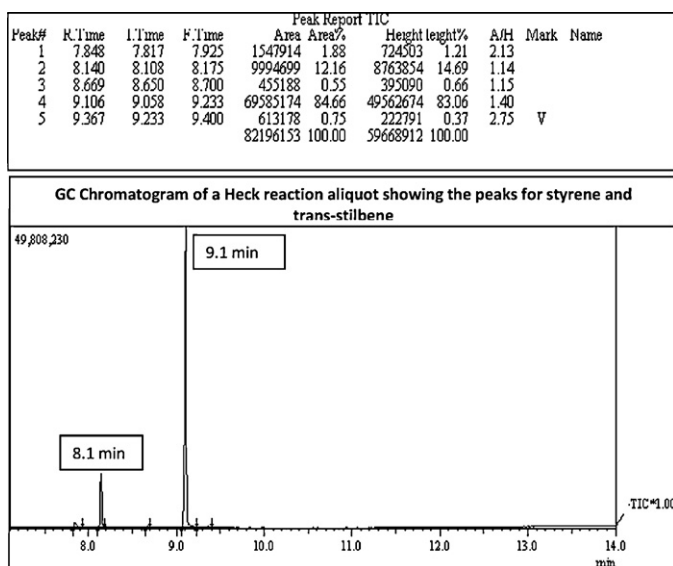


Fig. 12. Gas chromatogram trace for the Heck reaction reactants and products showing the retention times and peak areas; the peaks at 8.10 and 9.10 min represent styrene and trans-stilbene, respectively.

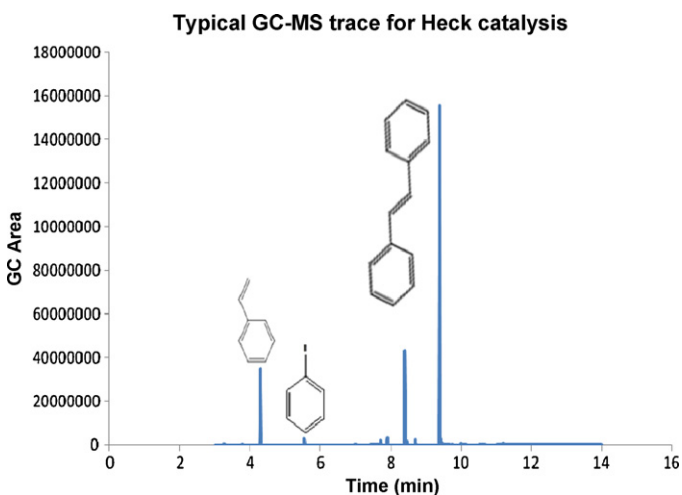


Fig. 13. Peak area for reactants and products obtained from the GC–MS trace.

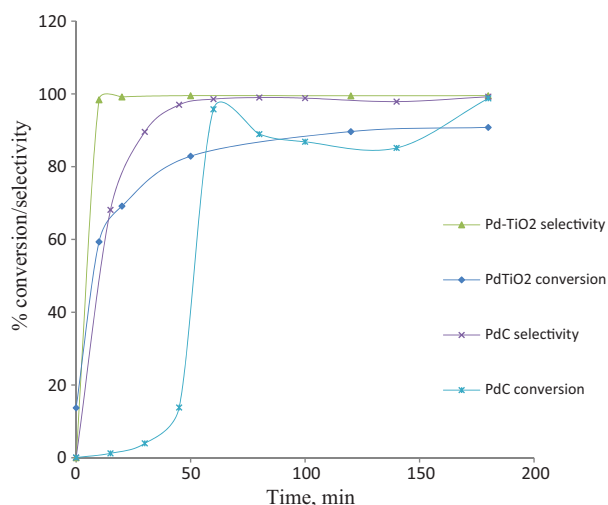


Fig. 14. Selectivity and conversion analysis of Pd–TiO₂ catalyst compared with Pd–C.

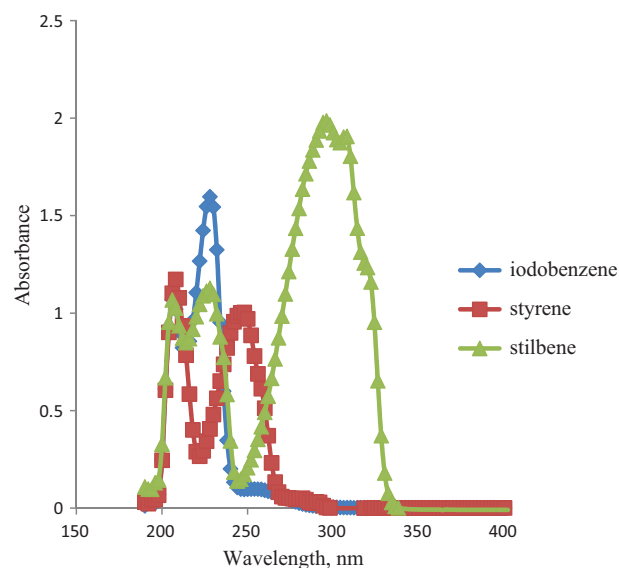


Fig. 15. Absorption spectra of the pure product and pure starting materials for the Heck reaction.

absorptions. The percent yield values were calculated relative to the molar absorptivity of the pure product. The absorbance of pure starting material and product was measured to obtain spectra that can be used to track the aliquots of the Heck reaction, Fig. 15. This provided a relatively quick and simple mode of analyzing the activity of the Pd–TiO₂ catalyst against various reaction conditions.

A Beer's law plot of several calibration standards of pure stilbene was generated by taking absorbance values at various known concentrations to obtain a molar absorptivity value of $26,590 \text{ M}^{-1} \text{ cm}^{-1}$ at a 296 nm operating wavelength, Figs. 16 and 17. At dilute concentrations, this value was subsequently used to calculate the exact concentration of stilbene in each aliquot for our Heck reaction series, assuming that the product peak at $\sim 296 \text{ nm}$ was for trans-stilbene. The accuracy of these values was confirmed by independent GC–MS analysis of the aliquots with minimal deviation.

3.2.4. NMR analysis of catalyst selectivity

Isolation and purification of the Heck catalysis product was not desired for this study, however pure product was isolated by re-

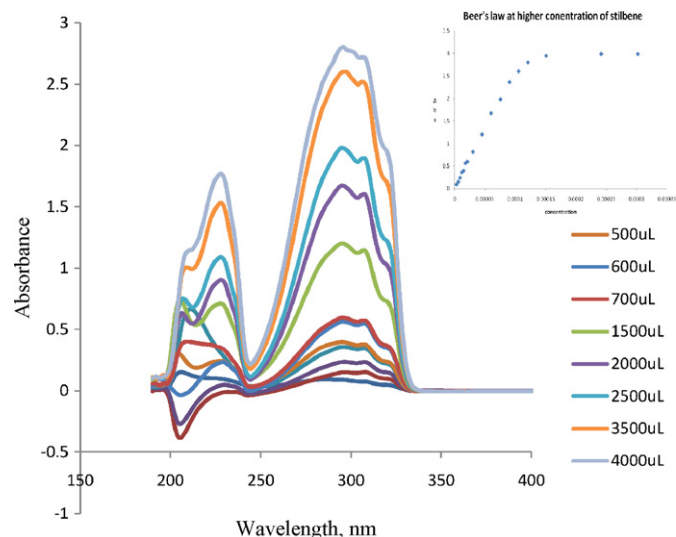


Fig. 16. Absorption spectra of known stilbene concentrations and inset, a Beer's plot showing deviation at higher concentrations.

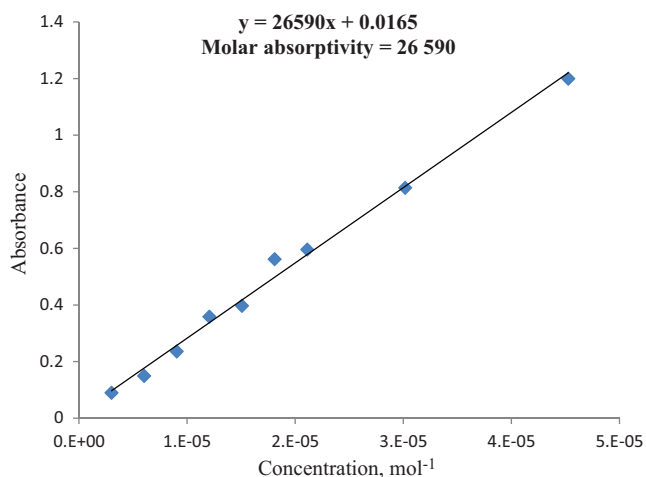


Fig. 17. Beer's plot to determine the molar absorptivity of stilbene diluted in methanol as the slope of the linear regression at an operating wavelength 296 nm, which is $26,590 \text{ M}^{-1} \text{ cm}^{-1}$.

crystallization from a mixture of dichloromethane and water. For a qualitative study, the pure product was then analyzed with ^1H NMR spectroscopy, Fig. 18. The singlet peak at 7.12 ppm was assigned to the vinyl protons whereas the peaks between 7.2 and 7.6 ppm were assigned to aromatic protons with varying chemical shift values depending on their proximity to the vinyl protons.

3.3. Catalyst optimization

3.3.1. Temperature effects on Heck reaction

A temperature range of 80–160 °C was used based on reported reaction temperature values obtained from the literature [17] for both the commercial Pd–C and the Pd–TiO₂ catalyst, Fig. 19. Pd–TiO₂ catalyst exhibited great stability at high reaction temperatures of upto 160 °C, Table 1. This can be attributed to thermal stability of the TiO₂ support thus enhanced catalyst activity at high reaction temperatures. Homogeneous Pd complexes would not be thermally stable at these temperatures [29,30] since high reaction temperatures rapidly convert the homogeneous Pd(II) species into Pd colloids which readily agglomerate in the absence of stabilizing molecules. Since oxidative addition of arylbromides and arylchlorides is slower, activation with Pd–TiO₂ catalyst, is expected at

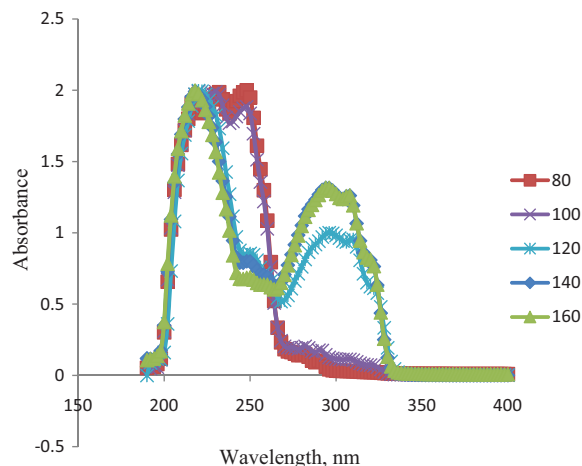


Fig. 19. Pd–iO₂ catalyst screening at varying temperatures.

Table 1

Temperature effects of 0.05 mol% Pd–TiO₂ on Heck coupling^a.

Temperature	80 °C	100 °C	120 °C	140 °C	160 °C
% Yield ^b	29	75	77	89	90

^a Yield of reaction between iodobenzene and styrene with Et₃N as base and 5 mL of NMP solvent.

^b Isolated yield of stilbene based on greater than 99% conversion of iodobenzene.

higher temperatures, with the utilization of stabilizing ligands such as tetrabutylammonium bromide.

3.3.2. Solvent effects on Heck reaction

The olefination of iodobenzene with styrene using Pd–TiO₂ catalyst and triethylamine as base, at 120 °C was used to study the effect of various solvents, Table 2. NMP, DMF, methanol and water were screened for their activity and selectivity in Heck reactions, Fig. 20.

The rates of reaction were found to be faster in polar aprotic solvents than in polar protic or non-polar solvents as confirmed by literature reports [31]. This could be attributed to the fact that methanol and water, being polar protic, are favorable for S_N1 substitution reactions and hence will consume the strong bases in a side reaction [32]. The removal of base from the reaction media inhibits

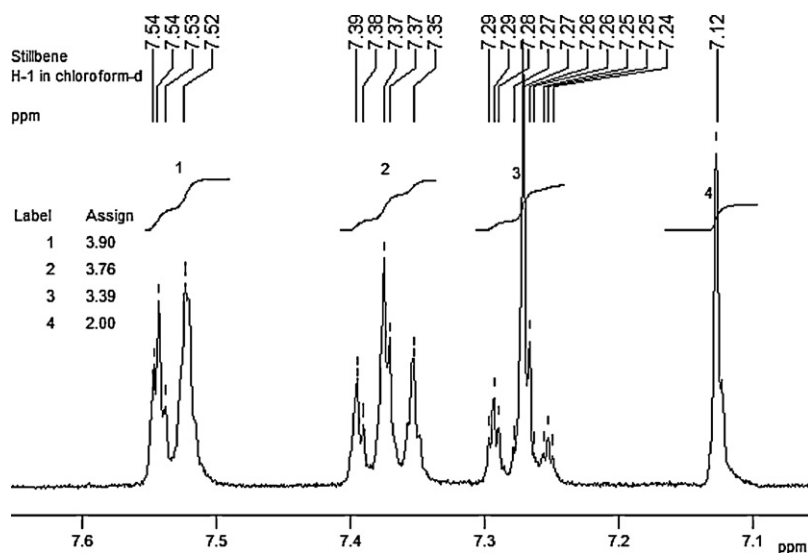


Fig. 18. NMR spectrum of trans-stilbene isolated and purified in a mixture of dichloromethane and water. This was further proof to the selective nature of the Pd–iO₂ catalyst.

Table 2
Solvent effects 0.05 mol% Pd–TiO₂ on Heck coupling^a.

Solvent ^c	NMP	DMF	DMAc	MeOH	Water
% Yield ^b	67.8	52.66	52.7	8.47	30.5

^a Yield of reaction between iodobenzene and styrene with Et₃N as base and at 120 °C.

^b Isolated yield of stilbene based on greater than 99% conversion of iodobenzene.

^c 5 mL of solvent was used in each case.

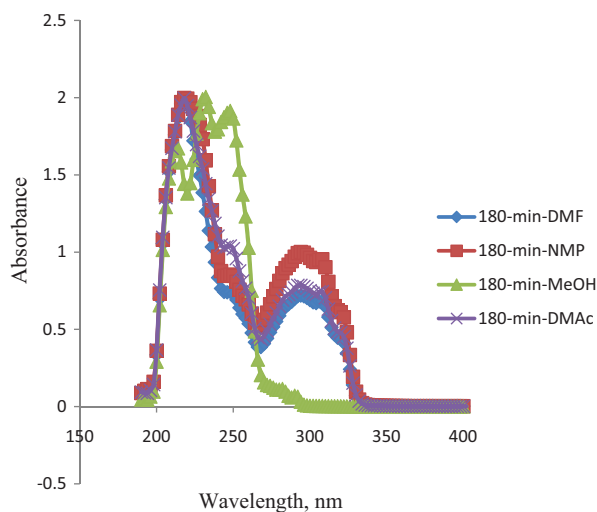


Fig. 20. Shows progression of reaction at 180 min reaction time using different solvents.

the Heck reaction mechanism. On the other hand, polar aprotic solvents are favorable for S_N2 substitution reactions, believed to be taking place in the proposed mechanism hence higher product yields. Uv–vis analysis indicated a red shift for the NMP reactions, Fig. 21, which can be attributed to the strong attractive polarization forces between the NMP solvent and the absorbing species. Though NMP was the best solvent for the Heck reactions (94% yield), DMF was considered as the optimum solvent considering the fact that the aliquots were to be used for further GC–MS and DCP–AES study. For GC–MS, NMP and iodobenzene have similar boiling points, the NMP peak therefore overlapped with iodobenzene peak hence poor resolution. For DCP–AES, NMP has a very high boiling point (202 °C) compared to DMF (153 °C), this hinders the disintegration process of the organics in the sample preparation step prior to DCP analysis.

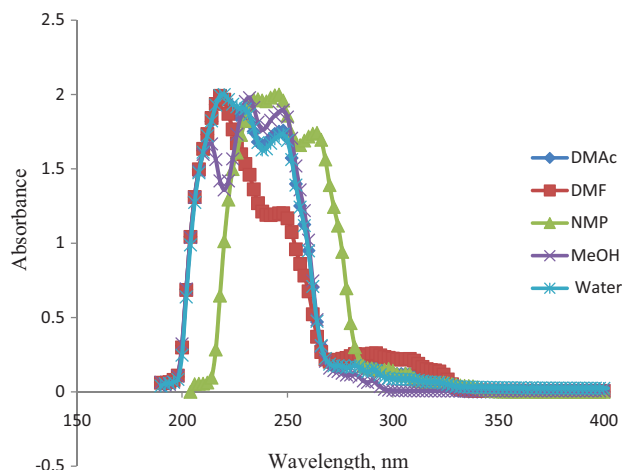


Fig. 21. Shows the NMP peak red shifted at 30 min.

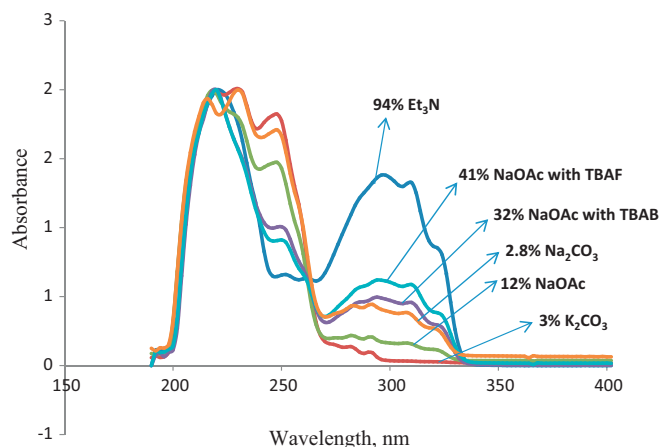


Fig. 22. Heck reaction screening with different bases.

3.3.3. Base effects on Heck reaction

A careful selection of base in terms of its solubility and basicity in the reaction mixture is extremely crucial. The role of the base in the mechanistic cycle is to re-activate the Pd species in solution, making it available to be recycled back into the reaction mixture [33]. This ensures a high turn-over frequency for the catalyst and in effect, high product yields. Based on literature reports, the following bases were expected to give good yields and were selected for the screening process NaOAc, Na₂CO₃ and K₂CO₃, Et₃N [33–35]. Contrary to literature reports, the inorganic bases recorded poor yields of trans-stilbene while triethylamine gave the highest yield, Fig. 22 and Table 3. This is likely due to relative insolubility effects of the inorganic bases in the organic reaction matrix. Phase transfer catalysts such as tetrabutylammonium bromide and tetrabutylammonium fluoride, significantly improved product yields for the inorganic bases. TBAF and TBAB are proposed to increase the solubility of the inorganic bases in the organic reaction matrix mainly by complex formation with the active Pd(II) ion in solution [35,36].

3.4. Catalyst activity

The surface area of available catalyst for Heck conversion of iodobenzene was determined using a BET analysis as described above. The TEM images were then used to estimate how many active sites were available on the TiO₂ surface based on the dispersion of Pd nanoparticles on TiO₂. From these results an optimized TOF value (number of moles of reacting substrate/(number of moles of active catalyst × time)) for the conversion of iodobenzene to trans-stilbene was found to be 7.85 min⁻¹.

3.5. Photoactivity of the Pd–TiO₂ catalyst

The photoactivity of the Pd–TiO₂ catalyst prepared by the method outlined in Section 2.4 was studied. After the catalyst was thoroughly dried in the oven at 120 °C for 3 h, two experiments were carried out. In the first experiment, the catalyst was used

Table 3
Base effects 0.05 mol% Pd–TiO₂ on Heck coupling^a.

Base	Et ₃ N	NaOAc	Na ₂ CO ₃	K ₂ CO ₃	NaOAc/TBAB ^c	NaOAc/TBAF ^c
% Yield ^b	94	12	2.9	3.0	32.6	41.6

^a Yield of reaction between iodobenzene and styrene with Et₃N as base and 5 mL of NMP.

^b Isolated yield of stilbene based on greater than 99% conversion of iodobenzene.

^c The ratio of NaOAc:TBAB and NaOAc:TBAF was 1:10 in both cases.

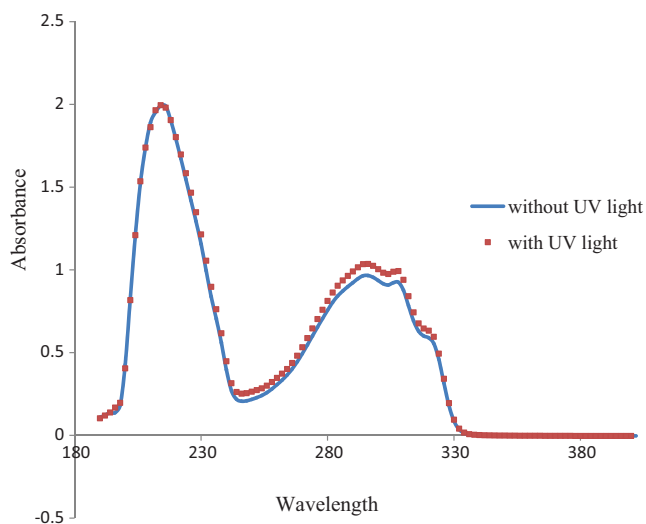


Fig. 23. Heck reaction analysis of Pd-TiO₂ catalyst to test for the effect of UV light irradiation during the conversion of iodobenzene. The Absorbance maximum peak at 296 nm shows a slight increase in stilbene production with UV light irradiation.

in a typical Heck reaction step with 0.5 mL iodobenzene, 0.614 mL styrene, 1 mL Et₃N and 5 mL DMF and left stirring at 140 °C for 2 h with UV light irradiation. In the second experiment the exact same reaction conditions were used, but without UV light irradiation. The analysis of the reaction aliquots for both experiments after 2 h suggest that the activity of the Pd-TiO₂ was improved only slightly under UV light irradiation, 62% yield, compared with, 57% yield, without UV light, Fig. 23. While the semiconductor nature of the titania nanofibers was successfully used to enhance catalyst formation, there was only limited increase in activity with UV light irradiation during the Heck reaction. It has been speculated that irradiation of titania can lead to the formation of highly reactive hydroxyl radicals which may be degrading starting material as well as inducing Heck coupling. More work is necessary to determine if this hypothesis is relevant.

3.6. Pd leaching effects on Heck reaction

A DCP-AES study for Pd leaching effects was carried out to find out the relative concentration of Pd²⁺ ions in solution with the progress of the reaction, Fig. 24. The percent of Pd²⁺ in solution, in relation to the amount of Pd used for the Heck reaction, was com-

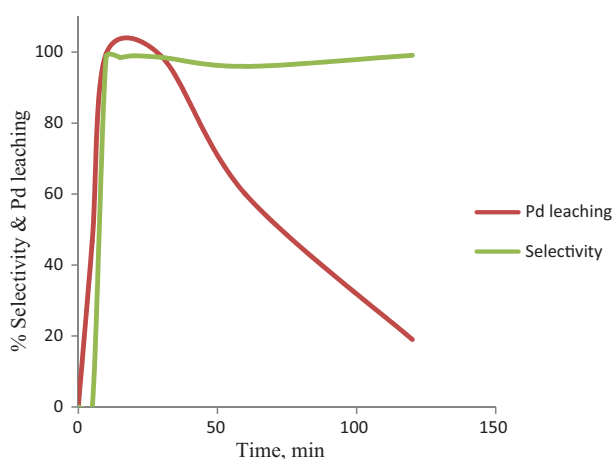


Fig. 24. DCP-AES results of Pd²⁺ ions in the reaction compared against product selectivity of the Pd-TiO₂ catalyst.



Fig. 25. Colour progression of the reaction aliquots with reaction time indicating the change in colour from grey, yellow and dark brown, which is consistent with the changes in oxidation state of the Pd species. (For interpretation of the references to color in this figure legend, the reader is referred to the web version of the article.)

pared against the selectivity of the catalyst with reaction time. The results indicated that at about 10 min reaction time, the Pd-TiO₂ catalyst was already ~100% selective for trans-stilbene with 99.5% Pd²⁺ ions in solution. The catalyst maintained its selectivity with reaction progress as the amount of Pd²⁺ ions decreased to almost zero at 120 min reaction time. As indicated in previous literature reports, presence of Pd²⁺ ions in the reaction mixture suggests that the Pd-TiO₂ catalyst is quasi-homogenous [16], where the Pd on the surface of TiO₂ would be oxidized to Pd²⁺ which will then drive the Heck reaction mechanism. Towards the end of the reaction, Pd would re-deposit onto the support when the aryl halide has been depleted, ready to take part in another cycle of reaction. The re-deposition of Pd on TiO₂ surface is consistent with the loss of Pd²⁺ ions concentration as the reaction progresses. TEM analysis of the Pd-TiO₂ catalyst taken after a Heck reaction mechanism indicated that the Pd nanoparticles remained anchored on the TiO₂ nanofiber surface and not leached in solution, thus allowing for re-use of the catalyst.

Reduction of the metal oxide supported catalyst could also be followed visually by observing the change in colour of the catalyst from yellow to brown-black, [20] Fig. 25. Initial aliquots of our reaction mixture exhibited a yellow colour indicating the oxidation of Pd⁰ to Pd²⁺. This is in-line with the oxidative addition of the aryl halide to the Pd⁰ complex. As the reaction progresses, the yellowish colour darkens to a brown-black colour indicating the re-deposition of the Pd²⁺ to Pd⁰ as the reaction comes to an end. The Pd-TiO₂ catalyst was further recycled in multiple Heck reaction cycles without loss of activity for the conversion of iodobenzene.

4. Conclusion

Photodeposition was successfully used for the first time to prepare a Pd nanoparticle catalyst on TiO₂ nanofibers supports. The newly developed catalyst was highly active with high Pd dispersion, small particle size of ~5 nm, and great thermal stability. The Pd nanoparticles remained stabilized on the electrospun titania under ambient conditions without degradation for extended periods of time. This photodeposition method is currently being utilized in the synthesis of tunable sizes and shapes of Group VIII metal nanoparticles on the TiO₂ surface.

The photodeposited Pd-TiO₂ catalyst gave 98% yield of trans-stilbene within 30 min reaction time. This value was significantly higher than the commercially available Pd-C catalyst which only

gave 80% yield after 60 min reaction time. The catalyst could be recycled with high efficiency and selectivity of up to 100% for the desired product with an optimized TOF value of 7.85 min⁻¹. Interestingly, results under UV photocatalyst conditions were only modestly successful in enhancing product yield. More work is necessary to explore how to better take advantage of the photoactivity of the TiO₂ nanofiber substrate.

Acknowledgments

Financial support for the conduction of this research was from PRF ACS-46117 grant. The funding body had no role in the preparation of the article. Prof. Dick Naslund at Geology Department, SUNY-Binghamton for DCP-AES work; Prof. David C. Doetschman and group at Chemistry Department, SUNY-Binghamton and Dr Thomas C. Keane, Abigail Feliciano & Meghan Flynn-Wilborn at Department of Chemistry and Biochemistry, Russell Sage College for GC-MS work; Dr In-tae Bae at S³IP (Small Scale Systems Integration and Packaging center), SUNY-Binghamton for TEM analysis.

References

- [1] Council for Chemical Research; Vision 2020 Catalysis Report, 1998.
- [2] C.H. Bartholomew, R.J. Farrauto, *Fundamentals of Industrial Catalytic Processes*, 2nd ed., Wiley-AIChE, 2005.
- [3] A. Suzuki, *Journal of Organometallic Chemistry* 576 (1999) 147–168.
- [4] J. Louie, J.F. Hartwig, *Tetrahedron Letters* 36 (1995) 3609–3612.
- [5] R. Narayanan, *Molecules* 15 (2010) 2124–2138.
- [6] Z. Li, J. Chen, W. Su, M. Hong, *Journal of Molecular Catalysis A: Chemical* 328 (2010) 93–98.
- [7] M. Sudip, R. Gadi, J. Ashutosh, B. Mubeen, S. Yoel, *Advanced Synthesis & Catalysis* 344 (2002) 348–354.
- [8] I. Pryjomska-Ray, A.M. Trzeciak, J.J. Ziolkowski, *Journal of Molecular Catalysis A-Chemical* 257 (2006) 3–8.
- [9] S. Shylesh, L. Wang, W.R. Thiel, *Advanced Synthesis & Catalysis* 352 (2010) 425–432.
- [10] K. Ferre-Filmon, L. Delaude, A. Demonceau, A.F. Noels, *Coordination Chemistry Reviews* 248 (2004) 2323–2336.
- [11] N.T.S. Phan, M. Van Der Sluys, C.W. Jones, *Advanced Synthesis & Catalysis* 348 (2006) 609–679.
- [12] K. Kohler, R.G. Heidenreich, J.G.E. Krauter, M. Pietsch, *Chemistry-A European Journal* 8 (2002) 622–631.
- [13] J. Salvadori, E. Balducci, S. Zaza, E. Petricci, M. Taddei, *Journal of Organic Chemistry* 75 (2010) 1841–1847.
- [14] U. Laska, C.G. Frost, G.J. Price, P.K. Plucinski, *Journal of Catalysis* 268 (2009) 318–328.
- [15] M.N. Alam, S.M. Sarkar, M.R. Miah, *Reaction Kinetics and Catalysis Letters* 98 (2009) 383–389.
- [16] K. Kohler, S.S. Prockl, W. Kleist, *Current Organic Chemistry* 10 (2006) 1585–1601.
- [17] J. Zhu, J.H. Zhou, T.J. Zhao, X.G. Zhou, D. Chen, W.K. Yuan, *Applied Catalysis A-General* 352 (2009) 243–250.
- [18] Y.J. Feng, L. Li, Y.S. Li, W.R. Zhao, J.L. Gu, J.L. Shi, *Journal of Molecular Catalysis A-Chemical* 322 (2010) 50–54.
- [19] V. Polshettiwar, C. Len, A. Fihri, *Coordination Chemistry Reviews* 253 (2009) 2599–2626.
- [20] C.M. Andersson, K. Karabelas, A. Hallberg, C. Andersson, *Journal of Organic Chemistry* 50 (1985) 3891–3895.
- [21] M.S. Hegde, G. Madras, K.C. Patil, *Accounts of Chemical Research* 42 (2009) 704–712.
- [22] A. Janbey, W. Clark, E. Noordally, S. Grimes, S. Tahir, *Chemosphere* 52 (2003) 1041–1046.
- [23] R.L. Augustine, S.T. O'Leary, *Journal of Molecular Catalysis A-Chemical* 95 (1995) 277–285.
- [24] K. Kohler, M. Wagner, L. Djakovitch, *Catalysis Today* 66 (2001) 105–114.
- [25] U. Diebold, S.C. Li, M. Schmid, *Annual Review of Physical Chemistry* Vol61 (61) (2010) 129–148.
- [26] O. Carp, C.L. Huisman, A. Reller, *Progress in Solid State Chemistry* 32 (2004) 33–177.
- [27] M.I. Litter, *Applied Catalysis B: Environmental* 23 (1999) 89–114.
- [28] H. Dong, S. Prasad, V. Nyame, W.E. Jones, *Chemistry of Materials* 16 (2004) 371–373.
- [29] T.N. Glasnov, S. Findenig, KappeF.C.O., *Chemistry-A European Journal* 15 (2009) 1001–1010.
- [30] F.Y. Zhao, B.M. Bhanage, M. Shirai, M. Arai, *Chemistry-A European Journal* 6 (2000) 843–848.
- [31] L. Djakovitch, H. Heise, K. Köhler, *Journal of Organometallic Chemistry* 584 (1999) 16–26.
- [32] M.G. Loudon, *Organic Chemistry*, 4th ed., Oxford University Press, 2002.
- [33] G.T. Crisp, *Chemical Society Reviews* 27 (1998) 427–436.
- [34] S. Mukhopadhyay, G. Rothenberg, A. Joshi, M. Baidossi, Y. Sasson, *Advanced Synthesis & Catalysis* 344 (2002) 348–354.
- [35] S.S. Prockl, W. Kleist, M.A. Gruber, K. Kohler, *Angewandte Chemie-International Edition* 43 (2004) 1881–1882.
- [36] M. Dams, L. Drijkoningen, B. Pauwels, G. Van Tendeloo, D.E. De Vos, P.A. Jacobs, *Journal of Catalysis* 209 (2002) 225–236.